A high specific capacity membraneless aluminum-air cell operated with an inorganic/organic hybrid electrolyte

Binbin Chen[a], Dennis Y.C. Leung[a,*], Jin Xuan[b], Huizhi Wang[b,*]

[a]Department of Mechanical Engineering, The University of Hong Kong, Pokfulam Road, Hong Kong

[b]School of Engineering and Physical Sciences, Heriot-Watt University, Edinburgh EH14 4AS, United Kingdom

*Corresponding authors, Tel.: +852 2859 7911, fax: +852 2858 5415, email: ycleung@hku.hk (D.Y.C. Leung); Tel: +44 (0) 131 451 8354; Fax: +44 (0)131 451 3129, email: h.wang@hw.ac.uk (H. Wang)

Abstract

Aluminum-air cells have attracted a lot of interests because they have the highest volumetric capacity density in theory among the different metal-air systems. To overcome the self-discharge issue of aluminum, a microfluidic aluminum-air cell working with KOH methanol-based anolyte was developed in this work. A specific capacity up to 2507 mAh g^{-1} (i.e. 84.1% of the theoretical value) was achieved experimentally. The KOH concentration and water content in the methanol-based anolyte were found to have direct influence on the cell performance. A possible mechanism of the aluminum reactions in KOH methanol-based electrolyte was proposed to explain the observed phenomenon.

Keywords

Aluminum-air cell

High specific capacity

Inorganic/organic hybrid electrolyte

Membraneless

Methanol-based anolyte

1. Introduction

Cost-effective and high-density energy storage remains an unmet demand for applications ranging from portable electronics to large-scale grid storage. Metal-air cells represent one of the prospective candidates for fulfilling this demand, as they inherit the highest energy content of all known batteries by integrating the inexhaustible ambient oxygen with the anode metals that possess a high ratio of valence electron to atomic nuclei [1, 2]. Among different anode metals, aluminum (Al) theoretically shows the highest volumetric capacity density (8.04 Ah cm^{-3} vs. 2.06 for lithium, 3.83 for magnesium and 5.85 for zinc) and a high specific capacity (2.98 Ah g^{-1} vs. 3.86 for lithium, 2.20 for magnesium and 0.82 for zinc) second only to lithium, thereby explaining the attention it has attracted [3]. Further advantages of the aluminum-air (Al-air) cell over other metal-air technologies include the abundance of anode raw materials, ease of handling, and excellent safety characteristics [4]. However, early developments of Al-air cell have achieved little commercial success, mainly due to the dependence on the use of aqueous electrolytes, which suffered severe self-discharge problems and resulted in practical energy densities inferior even to those of zinc-air systems [5]. An alternative idea of replacing the aqueous electrolytes with aprotic/organic ones has recently shown great promise by circumventing the conventional water-related problems, and has revived research activities on Al cells. Due to the low proton availability in the non-aqueous solvents, an almost complete inhibition of Al corrosion, and correspondingly, anode efficiency of nearly 100% have been demonstrated from half-cell experiments on the basis of methanol [6], ethanol [7], propanol [8], and ionic liquid electrolytes [9]. A big challenge, however, appears to be that most non-aqueous solvents will present difficulties when in contact with the air cathode,

which has seriously impeded the progress of full-cell development. Typical issues at the cathode of a non-aqueous metal-air cell include electrolyte decomposition by peroxide radical attack or other parasitic reactions with the catalytic electrode [10], cathode clogging by insoluble products [11, 12], and electrolyte contamination by absorbing ambient gases or moisture through the open structure of the gas diffusion cathode [13].

Non-aqueous/aqueous hybrid cell is an emerging technology to address the limitations of traditional single-electrolyte cell structures by operating electrodes in different electrolyte environments. The co-existence of both non-aqueous and aqueous solutions in a single cell is enabled with the incorporation of a solid layer made from materials such as LISICON [14], NASICON [15], and polymer [16]. The solid layer serves as both the membrane separator and the ion conductor between two different electrolytes. Feasibility of this concept has been successfully demonstrated in various prototypes, such as Li-air batteries [15, 17], Li-NiOOH batteries [18, 19], Li-AgO batteries, etc. [20]. Recent works have reported novel redox flow lithium batteries that employ an anolyte and a catholyte containing different redox mediators separated by a Nafion/PVDF membrane to achieve optimum performance [21, 22]. However, practical operations of these hybrid systems have generally shown low performance and a short life span due to intrinsic drawbacks of the solid separator including large ohmic resistance and poor chemical stability in strong alkaline or acidic environments [23].

To avoid the problems associated with the use of a solid separator, laminar flow-based microfluidic electrochemical cells have been extensively researched [24-26]. With a small ratio of inertial to viscous force, a laminar flow-based cell is able to maintain an interface between two streams of electrolytes, which acts as a virtual separator to prevent

the mixing of different electrolytes within the cell [27]. Yet, because most organic solvents have a very high affinity to form mixtures with water, a new membraneless strategy needs to be developed for an inorganic/organic hybrid electrolyte system.

This work reports a novel inorganic/organic hybrid electrolyte design for Al-air cell to achieve high specific capacity. The design eliminates the need for a solid-state separator by relying on a non-direct counter-flow microfluidic platform. Methanol was applied as an organic electrolyte solvent at the anode side, which has been shown to be an effective corrosion inhibitor for Al anodes [6, 28]. Traditional aqueous KOH electrolyte was applied at the cathode side. The interfacial mixing of the two electrolytes was visualized under different flow rates. The effects of KOH concentration and water content in the methanol-based anolyte on the cell performance were investigated. Post-discharge products of the cell were analyzed using XRD and FTIR, and reaction mechanisms in this newly-developed hybrid electrolyte cell were proposed. The cell design developed in this study can also be applicable to other metal-air systems.

2. Experimental

2.1 Chemicals

Alkaline electrolytes with different concentrations of KOH were prepared by dissolving KOH pellets (≥85%, Sigma-Aldrich, Hong Kong) in methanol (≥99.9%, Merck KGaA, Germany) and in 18 MΩ deionized water (Barnstead, NANOpure Diamond^{TM}, USA) under different test conditions. Commercial Al foil with an area density of 3.54 mg cm^{-2} was used as a cost-effective anode. The compositions of the foil were analyzed by energy-dispersive X-ray on a Hitachi S-4800 microscope to have 99.0% purity of Al with

trace amounts of Fe and Ag as impurities. A gas diffusion electrode (GDE, Hesen Company, China) with a catalyst loading of 2 mg cm^{-2} Pt/C (Johnson Matthey, USA) was adopted as the air cathode for oxygen reduction.

2.2 Cell fabrication and assembly

The cell consisted of three polyvinyl chloride (PVC) layers cut out by a carbon dioxide laser ablation system (VLS 2.30, Universal Laser System, USA). The top layer contained two inlets and one outlet for electrolyte flows. The two inlets were respectively connected to the anolyte sub-channel and catholyte sub-channel cut out on the second layer. On the third (bottom) layer, two square windows were cut out to allow the electrodes to contact with the electrolytes. The active projected electrode area was 0.015 cm^2, and all current and power densities were normalized by this area. The distance between the anode and the cathode was 2.0 mm. The three layers had thicknesses of 0.1 mm, 0.5 mm, and 0.1 mm, respectively, and they were bound together using double-side adhesive tape. The electrolyte was pumped into the cell by a syringe pump (LSP02-1B, LongerPump, China), via 1.5 mm tubing bonded to the ports with epoxy. Copper foil was used as a current collector to connect the electrodes to an external circuit.

2.3 Fluorescent dye characterization

Solutions of bromophenol blue ($C_{19}H_{10}O_5Br_4$), a methanol/water-ratio-sensitive dye, were prepared with a concentration of 1.75 mg mL^{-1} in solvents containing different volume ratios of methanol and deionized water. The solutions were observed by Precentered Fiber Illuminator (Intensilight C-HGFI Nikon, Japan) using yellow fluorescent

light with a wavelength ranging between 600 and 630 nm. At this wavelength range, the methanol solution of $C_{19}H_{10}O_5Br_4$ is a transparent orange solution, while its water solution is opaque. The color is gradually transformed when the volume ratios of methanol/water changed. For calibration, the colors of $C_{19}H_{10}O_5Br_4$ solutions with different methanol/water volume ratios were captured by the Illuminator. Then, pure $C_{19}H_{10}O_5Br_4$ methanol solution and water solution were pumped into the cell channel structure to investigate the flow pattern of methanol and water electrolytes at different flow rates.

2.4 Electrochemistry

Electrochemical measurements were conducted under room conditions. The polarization curves were obtained by potentiostatic current measurement at every 0.2 V for 200s to reach a steady state, from open-circuit voltage (OCV) to 0 V, by an electrochemical workstation (CHI 660E, Shanghai Chenhua Instruments Co., Ltd., China). The average value of the current data in the last 50 seconds of the sampling was used to represent the cell current at a certain voltage. An external Ag/AgCl (in saturated KCl) electrode (Shanghai Lei-ci Co., Ltd., China) was used as a reference electrode to acquire the single-electrode potentials of the cells. The potential data was recorded in situ by a digital multi-meter (15B, Fluke Corporation, USA). Electrochemical impedance spectroscopy (EIS) tests were taken in the frequency range of 120 kHz-5 mHz with an A.C. amplitude of 5 mV at 0.8 V, which was around the peak-power voltage.

To evaluate the specific capacity of Al in the cell discharged at a small current density, where Al suffered serious corrosion, galvanostatic discharging was performed at a current of 0.015 mA, corresponding to a current density of 1.0 mA cm^{-2}. The specific capacity (C)

and Coulombic efficiency (ɳ) of Al were calculated as:

$$C = \frac{I \cdot t}{M}\ , \qquad (1)$$

$$\eta = \frac{C}{C_{th}}, \qquad (2)$$

where I is the discharging current used (i.e. 0.015 mA), t is the discharging time (h), M is the mass of Al consumed (M=53×10^{-6} g in this study), and C_{th} is the theoretic specific capacity of Al (2980 mAh g^{-1}).

2.5 Post-discharge characterization

Post-discharge products precipitated on the Al surface were first cleaned with methanol. They were then dried and ground into powder for X-ray diffusion (XRD) analysis (D8 ADVANCE Diffractometer, Bruker AXS, USA) with Lynxeye detector Cu/Kα radiation operating at 40 kV/40 mA. The products were identified based on the database in the JADE diffraction analysis software (Material Data Inc., USA). The residual methanol-based electrolyte solution was taken out and dried by a rotary evaporator (Rotavapor R-210, BUCHI, Switzerland) to remove the methanol and form white powders. As a control group, 20 mL of 2 M KOH methanol-based solution was dried under the same condition to remove the methanol solvent, forming KOH powders. The powder samples from these two solutions were made into KBr pellets with a 13 mm diameter for Fourier transform infrared spectroscopy (FTIR) analysis (IRAffinity-1s, Shimadzu Co., Japan) to verify whether any other organic product was generated.

3. Results and Discussion

3.1 Design principle and chemical patterns

The cell design is based on a non-direct counter-flow microfluidic platform as shown in Figure 1(a). Figure 1(b) shows the visualization optical micrographs of methanol- and water-based electrolyte flow pattern in this cell structure as a function of flow rates, from 100 μL min^{-1} to 1000 μL min^{-1}. A mixing segment can be easily observed in the middle part. As the flow rate increased, the influence of convective flux became greater than the opposite diffusive mixing flux, shrinking the mixing segment of the electrolyte in this counter-flow architecture. At a flow rate of 1000 μL min^{-1}, the boundary of the diffusion segment was restricted within the range between the two electrodes (electrode areas are denoted by the red squares), indicating that there was minimal crossover of electrolytes to the opposite electrode. Figure 1 (c) shows the photograph of the developed hybrid electrolyte Al-air cell.

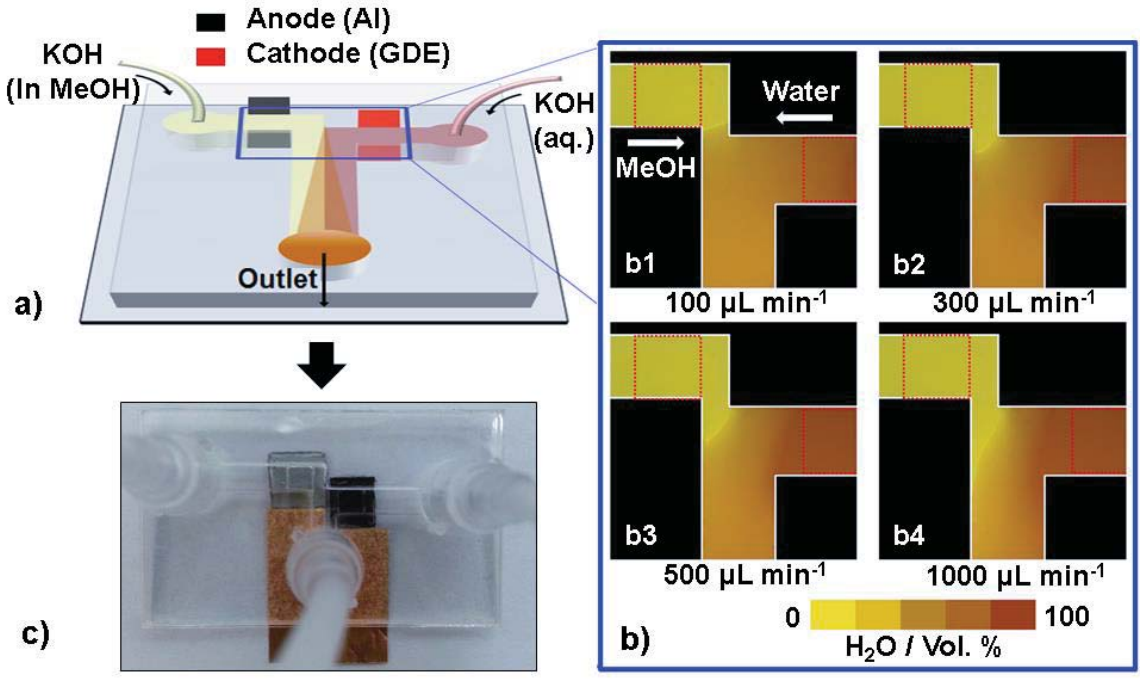

Figure 1 (a) Schematic of the hybrid electrolyte Al-air cell built on a non-direct counter-flow microfluidic platform. (b) Electrolyte flow pattern within the cell at a stream flow rate

of (b1) 100 μL min^{-1} (b2) 300 μL min^{-1} (b3) 500 μL min^{-1} and (b4) 1000 μL min^{-1}. The contours reflect the water content inside the cell captured by a fluorescent microscope, flowing neat methanol and deionized water side by side. (c) Photograph of a hybrid electrolyte Al-air cell.

3.2 Electrochemical performance

3.2.1 Discharge characteristics

Figure 2 shows the cell performance and individual electrode polarization curves as a function of KOH concentration and water content in the methanol-based anolyte. As shown in Figure 2(a) and (b), the cell with 1 M KOH in the electrolyte had an OCV of 1.36 V, with the anodic and cathodic potential of -1.31 V and 0.05 V vs. Ag/AgCl, respectively. When the KOH concentration increased to 4 M, the OCV increased to 1.59 V. Further examination on the individual electrode polarizations in Figure 2 (b) showed that the OCV increase was mainly due to the improvement of the anodic potential, which shifted to –1.57 V vs. Ag/AgCl as KOH concentration increased to 4 M. The shift of the anodic potential with KOH concentration could be explained by the Nernst equation where the electrode potential was a function of OH^- concentration. The increase of KOH concentration could also increase the electrolyte conductivity and mass transfer, thereby improving the cell performance [29]. However, the current density was found to be limited at lower voltages. The cell with 3 M KOH electrolyte showed the highest short-circuit current density of 8.63 mA cm^{-2}.

As shown in Figure 2(c) and (d), the water percentage in the anolyte had slight influence on the OCV (1.45 ± 0.05 V). However, the polarization curves in Figure 2(c)

showed an increase in cell output with higher water content. The short-circuit current density sharply increased from 1.25 mA cm^{-2} in the 0% case to 51.59 mA cm^{-2} in the 60% case. This indicates that the electrochemical performance of the cell was significantly improved with increasing water content in the methanol-based anolyte. The performance improvement was attributed to (i) enhanced mass transfer with decreased viscosity of the electrolyte solution; (ii) activation of the dissolution process of the passive film on Al surface after discharging; and (iii) improvement of the conductivity of the electrolyte solution. As reflected from the individual electrode polarization curves, the cell performance was limited by the Al anode rather than the air cathode.

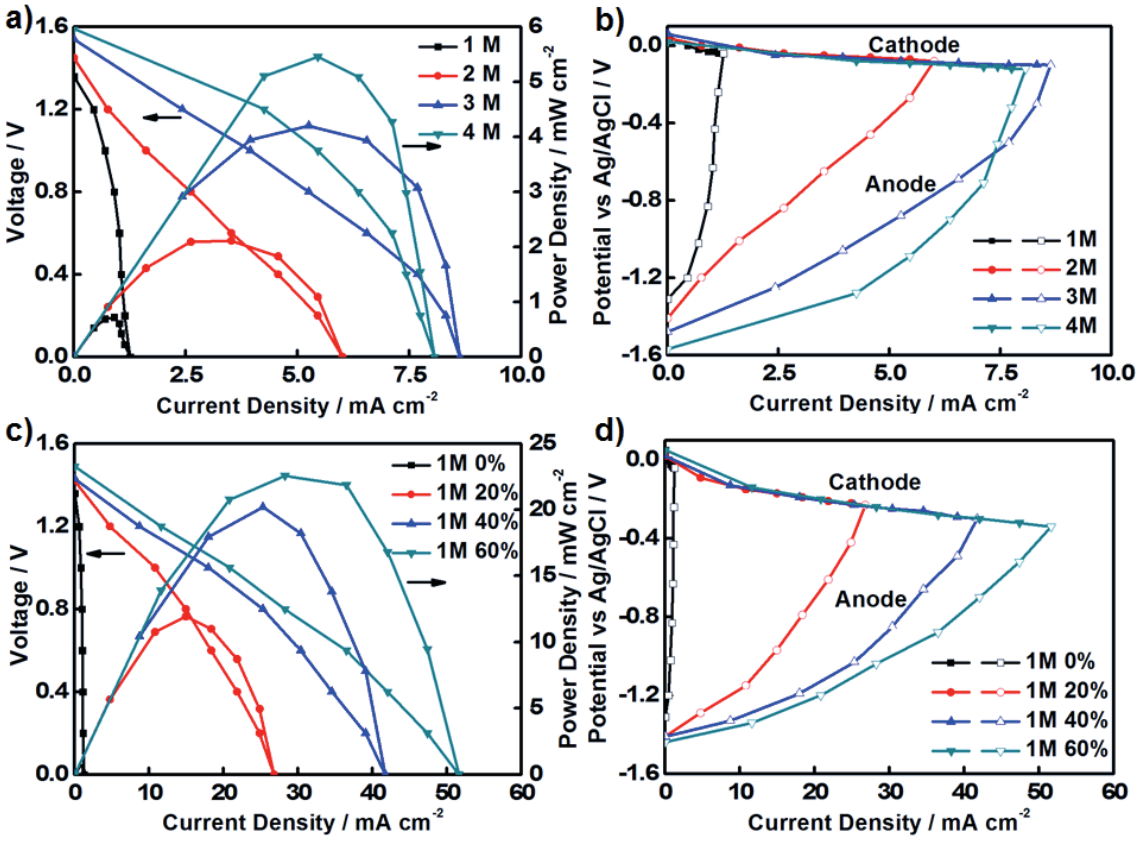

Figure 2 (a) Cell performance curves and (b) individual electrode polarization curves of

the hybrid electrolyte Al-air cells with different KOH concentrations (Anolyte: neat methanol-based KOH solutions with KOH concentrations of 1 M, 2 M, 3 M and 4 M; Catholyte: aqueous KOH solution with KOH concentrations of 1 M, 2 M, 3 M and 4 M. (c) Cell performance curves and (d) individual electrode polarization curves of the hybrid electrolyte Al-air cells with different water content in the anolyte (Anolyte: 1 M KOH methanol-based solution with various water contents of 0 vol.%, 20 vol.%, 40 vol.% and 60 vol.%; Catholyte: 1 M KOH aqueous solution).

Discharge curves of the Al-air cells are plotted in Figure 3. In this figure, the discharge curves of the Al-air cell with methanol-based anolyte indicate that Al exhibited much higher Coulombic efficiencies in the methanol-based anolytes than in the water-based ones, which is consistent with the findings of Wang et al. [28]. In fact, hydrogen generation was barely observed in the cell with methanol-based anolyte, indicating that the parasitic reaction was almost suppressed completely. At a discharge current density of 1.0 mA cm^{-2}, the Al-air cell achieved the highest specific capacity of 2507 mAh g^{-1} with 1 M electrolyte, corresponding to a Coulombic efficiency of 84.1%, which is one of the highest values achieved to date for Al anodes [28, 30-32]. By multiplying the specific capacity with the voltage, an energy density of 3004 mWh g^{-1}-anode (8080 mWh cm^{-3}-anode) was achieved by the cell with 1 M KOH methanol-based anolyte containing 20 vol% of water, which was 4 times that of the state-of-the-art in Zn-air batteries (741 mW g^{-1}-anode) [33]. Recent work has shown that a Na-air cell can achieve an energy density of 2087 mW g^{-1}-anode [34], which is the highest value reported in literature for metal-air batteries so far. The present hybrid electrolyte Al-air cell outperforms it, due to the advantage of the Al anode in specific capacity benefiting from its inherent tri-valence property.

As shown in Figure 3, under the same discharge current of 1 mA cm^{-2}, the voltage of the cells increased with increasing KOH concentration and anolyte water content, which is consistent with the performance curves in Figure 2. Meanwhile, the voltage profiles during each discharge fluctuated because of the competing process of passive layer generation and the increment of reaction area on the Al surface [35]. On the other hand, increased in KOH concentration and anolyte water content decreased the capacity. By increasing the KOH concentration from 1 M to 4 M, the specific capacity of Al decreased from 2507 mAh g^{-1} to 1330 mAh g^{-1}. Also, by increasing the water content from 0% to 20%, 40%, and then 60%, the specific capacity dropped from 2507 mAh g^{-1} to 2146 mAh g^{-1}, 999 mAh g^{-1}, and 663 mAh g^{-1}, respectively. This drop in specific capacity with increasing water content is due to the higher aluminum corrosion rate in the anolyte with higher water content as water was directly involved in the corrosion process of aluminum. To further understand the effects of KOH concentration on the specific capacity, the reaction mechanisms were investigated and detailed in Section 3.3.

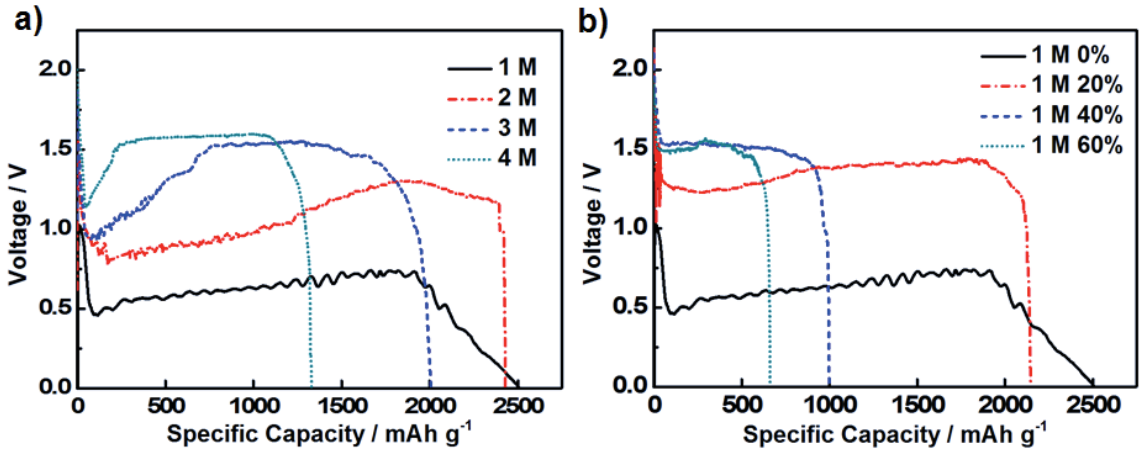

Figure 3 Specific capacities of Al foil in the hybrid electrolyte Al-air cells with (a) anolyte: neat methanol-based KOH solutions with KOH concentrations of 1 M, 2 M, 3 M and 4 M;

catholyte: aqueous KOH solution with KOH concentrations of 1 M, 2 M, 3 M and 4 M. (b) anolyte: 1 M KOH methanol-based solution with various water contents of 0 vol.%, 20 vol.%, 40 vol.% and 60 vol.%; catholyte: 1 M KOH aqueous solution.

3.2.2 Impedance spectroscopy

Nyquist plots of the Al-air cell working with different anolytes are shown in Figure 4(a) and (b). The equivalent circuit for the impedance of Al-air cells working in alkaline environment is shown in Figure 4(c). It consists of anodic and cathodic sections as detailed in our previous study [36]. The first step of anodic dissolution of Al (i.e. the consumption of Al and the formation of Al^{+} ion) contributes to a high-frequency capacitive loop. Middle-frequency inductive response appears due to the adsorption process of intermediates (such as OH^{-} or O^{2-}) [37]. At last, the growth and dissolution of the hydrous surface film ($Al^{+} \rightarrow Al^{3+}$, and $Al(OH)_3 \rightarrow Al(OH)_4^{-}$) result in a low-frequency loop [38]. For the cathode side, the high–frequency and low-frequency impedance respectively reflect a capacitance in the catalyst layer and the kinetic impedance of the oxygen reduction reaction [39]. The definitions of each element in the equivalent circuit are listed in Table 1.

As can be seen in Figure 4(a) and (b), cells with anolyte of neat methanol-based KOH solutions feature EIS curves with a high-frequency capacitive loop, a middle-frequency inductive loop, and a low-frequency line (Figure 4(a)), while the line at low frequency changes to a capacitive loop when water exists (Figure 4(b)). As there is no change in the reaction mechanism, the low-frequency line corresponds to the beginning section of the semi-circle loop. The fitting values of different resistances in equivalent circuit are list in Table 2.

The intercept on the x-axis of the EIS curves at high frequency, corresponding to the internal cell resistance ($\mathbf{R_{cell} = R_E + R_{Bulk}}$), slightly depended on the concentrations of KOH in the methanol-based anolyte. However, it decreased significantly with the increase of water content, indicating a lower solution resistance for electrolyte containing water. The phenomenon was mainly due to the improvement of solution conductivity with increasing water content. With the increase of KOH concentration and water content, the resistance values decreased significantly, which was consistent with the observed decreased diameters of the high-, middle- and low-frequency loops in the EIS curves. The transition between the EIS curves for cells with KOH methanol-based anolyte and with water-based anolyte was mainly due to the decreased resistance of $\mathbf{R_c}$, corresponding to the growth and dissolution of the hydrous surface film, which was further supported by the SEM observation in Figure 5.

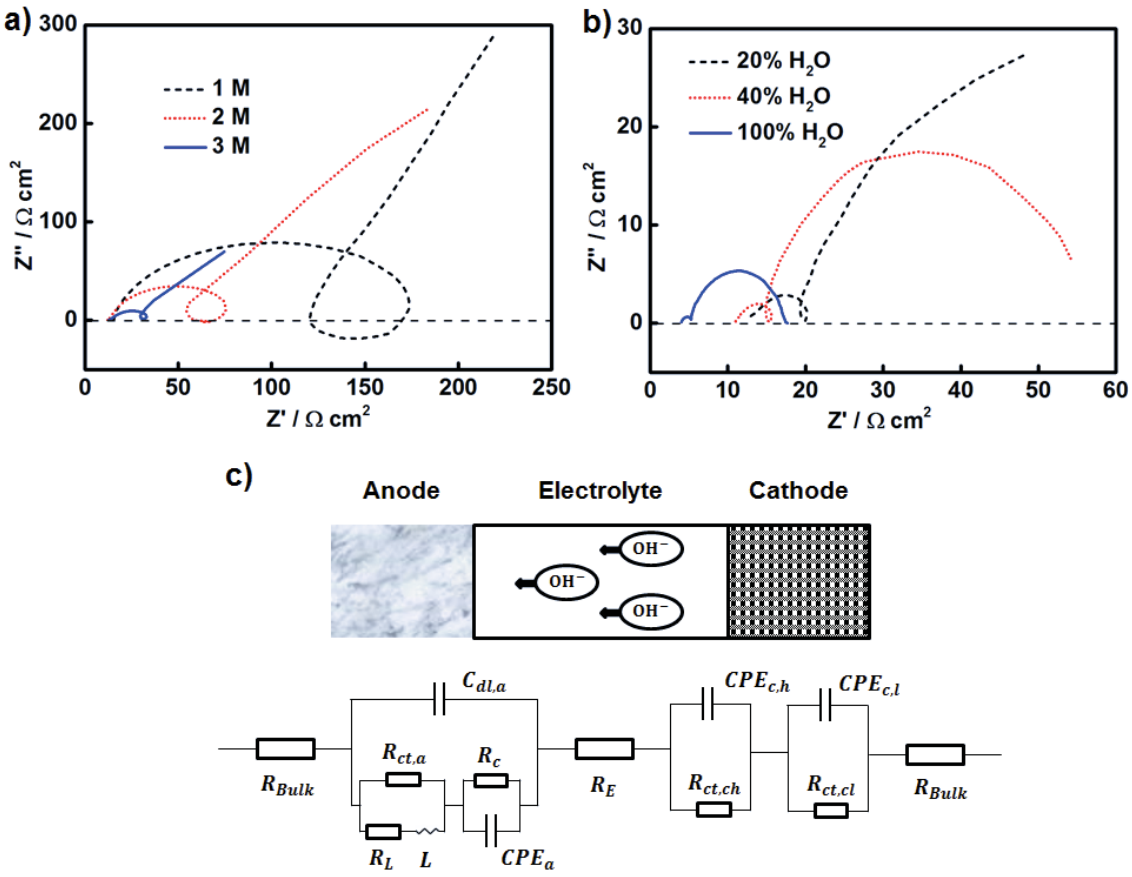

Figure 4 Impedance diagrams of the hybrid electrolyte Al-air cells with (a)anolyte: neat methanol-based KOH solutions with KOH concentrations of 1 M, 2 M and 3 M; catholyte: aqueous KOH solution with KOH concentrations of 1 M, 2 M and 3 M; (b) anolyte: 1 M KOH methanol-based solution with various water contents of 20 vol.%, 40 vol.% and 100 vol.%; catholyte: 1 M KOH aqueous solution. (c) Schematic of an alkaline Al-air cell and its equivalent circuit.

Table 1 Definition of each element in the equivalent circuit shown in Figure 4 (c).

R_E	Electrolyte ohmic resistance	R_{Bulk}	Resistance of electrode bulk and contacting

$C_{dl,a}$	Double-layer capacitance due to the first step of anode oxidation	$R_{ct,a}$	Charge transfer resistance due to the first step of anode oxidation
L	Inductance of adsorption on anode side	R_L	Resistance of adsorption on anode side
CPE_a	Constant phase element due to growth and dissolution of hydrous layer on anode side	R_c	Charge transfer resistance due to growth and dissolution of hydrous layer on anode side
$CPE_{c,h}$	Constant phase element due to the high-frequency response of cathode side	$R_{ct,ch}$	Charge transfer resistance due to the high-frequency response of cathode side
$CPE_{c,l}$	Constant phase element due to the low-frequency response of cathode side	$R_{ct,cl}$	Charge transfer resistance due to the low-frequency response of cathode side

Table 2 Fitting results of EIS curves in Figure 4.

Ω cm^{-2}	R_{cell}	$R_{ct,a}$	R_L	R_c	$R_{ct,ch}$	$R_{ct,cl}$
1 M	16.24	158.4	212.8	1806	2.68	28.64
2 M	11.35	69.31	84.02	1067	1.68	19.25
3 M	12.67	19.95	35.18	302.8	0.83	14.38
20 %	13.45	4.50	30.57	75.3	2.88	27.83
40 %	11.32	1.80	19.12	38.5	2.57	26.83
100 %	4.00	0.61	2.35	12.8	2.65	28.74

3.3 Reaction mechanism

Methanol is not corrosive to most metals. A moderate corrosion rate of methanol on Al with an order of 1-10 mils (25-250 μm) per year has been measured by Ferrando [40]. This characteristic shows that Al corrosion in conventional water-based electrolyte could be significantly inhibited by using a methanol-based anolyte. However, when KOH concentration and water content in the anolyte increase, the capacity densities of Al will decrease, indicating the aggravation of corrosion reaction. This section investigates the reaction mechanisms of Al in KOH methanol-based anolyte, including discharge and corrosion reactions.

3.3.1 Surface morphology

The morphologies of the Al surface after discharging in KOH neat methanol-based and water-based anolyte are shown in Figure 5. A rough surface configuration was formed on the discharged anode surfaces in both cases, while a significant difference between the two cases can be easily observed. The pore size of the Al discharged in the water-based anolyte was much larger than that of Al discharged in the methanol-based anolyte. This was due to the increase in the rate of dissolution of Al hydroxide layer. This could also be seen in their sectional views. The surface of Al discharged in methanol-based anolyte was covered by a passive layer, while Al discharged in water-based anolyte showed a sharp edge on the surface, indicating a higher dissolution rate of this passive film. Previous researchers have studied the influences of the passive layer and Al surface morphology on impedance [41-43]. Surface roughening has been identified as a reason for the

intermediate-frequency inductive loop, while the growth of a surface film resulting in high polarization resistance leads to a large low-frequency loop [38]. This is consistent with the EIS results presented in section 3.2.2 and accounts for the difference between the EIS curves of Al-air cells working with methanol- and water-based anolyte.

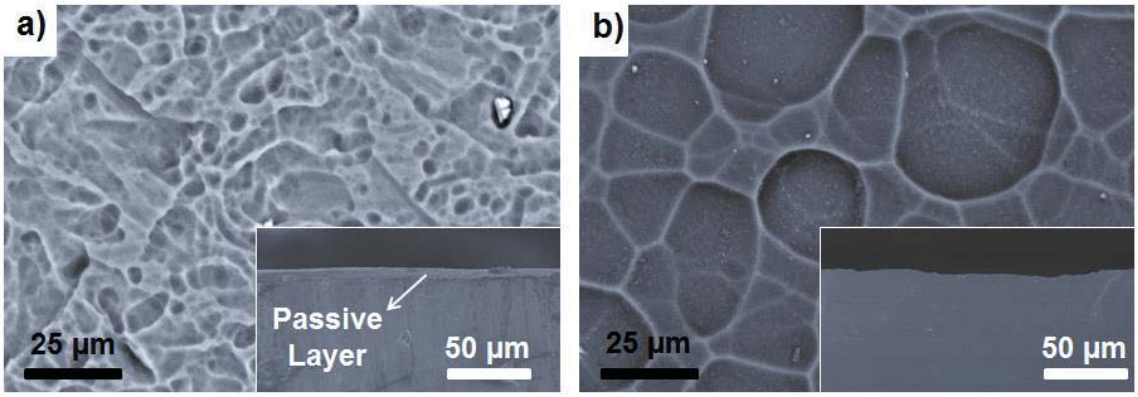

Figure 5 SEM images of Al surface morphologies after discharging in (a) neat methanol-based and (b) water-based KOH anolyte. Insets are the corresponding sectional views of the Al electrodes.

3.3.2 Discharge mechanism

The XRD pattern of the precipitates after discharging is shown in Figure 6. The main products corresponded to a mix of $Al(OH)_3$ and $K_2CO_3(H_2O)_{1.5}$. Referring to Al, $Al(OH)_3$ was the most common discharged product. Considering the high specific capacity that Al achieved, the main reaction between Al and KOH methanol-based solution is:

$$Al + 3OH^- \rightarrow Al(OH)_3 + 3e^- \quad (3)$$

Therefore, the discharge reaction of Al in KOH methanol-based solution is the same as that in KOH water-based solution. Additional $K_2CO_3(H_2O)_{1.5}$ might come from the impurities

of KOH samples and the reaction between KOH and the CO_2 from the air [44].

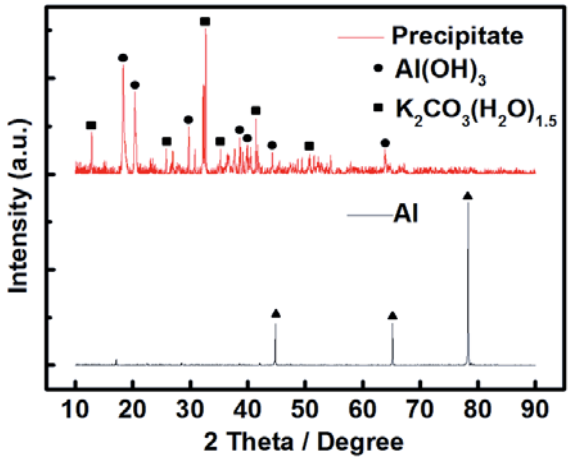

Figure 6 XRD pattern of the precipitate on Al surface after discharging in KOH methanol-based anolyte, comparing with XRD signals of pure Al. Major peaks are marked.

3.3.3 Corrosion mechanism

In an alcohol-based alkaline solution, alkoxide is a potential product as a result of the reversible reaction of metal oxides or hydroxides with alcohol [45]. In a KOH methanol-based solution, an equilibrium reaction exists as following:

$$KOH + CH_3OH \leftrightarrow CH_3OK + H_2O \quad (4)$$

Due to the existence of water, the corrosion reaction of Al will happen as:

$$Al + 3H_2O \rightarrow Al(OH)_3 + \frac{3}{2}H_2 \uparrow \quad (5)$$

Increasing KOH concentration drives Equation (4) to the product side, resulting in higher water content and accelerating the corrosion reaction rate. This explains the decrease of specific capacity of Al in KOH methanol-based solution with higher concentrations. Therefore, the total corrosion reaction of Al in KOH methanol-based solution is:

$$2Al + 6KOH + 6CH_3OH \rightarrow 2\,Al(OH)_3 + 6KCH_3O + 3H_2\uparrow \qquad (6)$$

To investigate whether there are more complex organic products, the powder samples are extracted from the KOH methanol-based solution with and without Al discharging and made into KBr pellets for FTIR analysis. The infrared scanning of the two samples shows the same results of FTIR spectra as shown in Figure 7 and Table 3, indicating there are no other complex organic compounds generated.

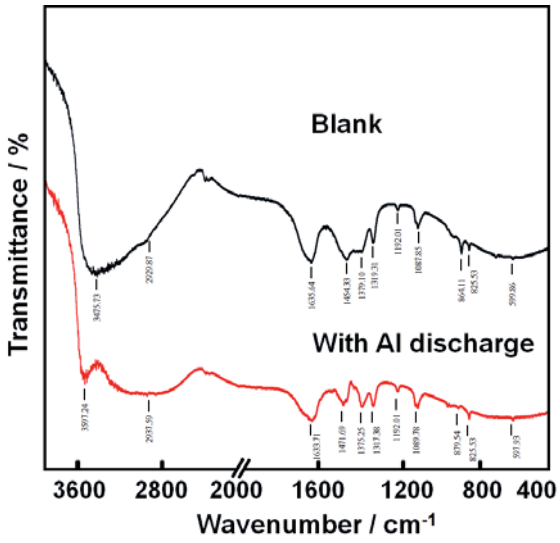

Figure 7 FTIR spectra of the powder samples obtained from KOH methanol-based solution without/with Al discharge.

Table 3 Positions of FTIR characteristic bands shown in Figure 7.

	Infrared active band position / cm $^{-1}$					
Blank	3475.73	2929.87	1635.64	1454.33	1379.1	1319.31
With Al discharge	3597.24	2937.59	1633.71	1471.69	1375.25	1317.38

Blank	1192.01	1087.85	864.11	825.53	599.86
With Al discharge	1192.01	1089.78	879.54	825.53	597.93

4. Conclusions

This work studied the characteristics of an Al-air cell working with methanol-based anolyte. The cell was built on a non-direct counter-flow microfluidic cell platform to avoid the use of an expensive membrane. The inhibition of crossover between different electrolytes was verified first by observing the flow pattern of methanol and water in the cell channel. The influences of electrolyte concentration and water content on cell performances were then investigated. The capacity tests showed that the self-corrosion of Al could be effectively inhibited by using KOH methanol-based solution as anolyte. Under this operation, the Al-air cell achieved a high specific capacity with low-cost commercial Al foil. In the experiment, the highest specific capacity of 2507 mAh g^{-1} was achieved (84.1% of the theoretical value), which is among the highest values achieved to date. In the last section, the reaction mechanisms of Al in a KOH methanol-based solution were investigated for the first time.

Acknowledgement

The authors would like to acknowledge the financial support from the Hong Kong Research Grant Council GRF#714313 and SRT on Clean Energy of the University of Hong Kong.

Reference

[1] J.S. Lee, S. Tai Kim, R. Cao, N.S. Choi, M. Liu, K.T. Lee, J. Cho, Advanced Energy Materials, 1 (2011) 34-50.

[2] R.S. Jayashree, L. Gancs, E.R. Choban, A. Primak, D. Natarajan, L.J. Markoski, P.J. Kenis, J. Am. Chem. Soc., 127 (2005) 16758-16759.

[3] Q. Li, N.J. Bjerrum, J. Power Sources, 110 (2002) 1-10.

[4] E. Shkolnikov, A. Zhuk, M. Vlaskin, Renewable and Sustainable Energy Reviews, 15 (2011) 4611-4623.

[5] D. Egan, C.P. De León, R. Wood, R. Jones, K. Stokes, F. Walsh, J. Power Sources, 236 (2013) 293-310.

[6] J. Wang, J. Wang, H. Shao, X. Chang, L. Wang, J. Zhang, C. Cao, Materials and corrosion, 60 (2009) 269-273.

[7] H. Shao, J. Wang, X. Wang, J. Zhang, C. Cao, Electrochem. Commun., 6 (2004) 6-9.

[8] A. Mukherjee, I.N. Basumallick, J. Power Sources, 58 (1996) 183-187.

[9] T. Hibino, K. Kobayashi, M. Nagao, Journal of Materials Chemistry A, 1 (2013) 14844-14848.

[10] P. Kichambare, J. Kumar, S. Rodrigues, B. Kumar, J. Power Sources, 196 (2011) 3310-3316.

[11] J. Yuan, J.-S. Yu, B. Sundén, J. Power Sources, 278 (2015) 352-369.

[12] Y.G. Zhu, X. Wang, C. Jia, J. Yang, Q. Wang, ACS Catalysis, (2016).

[13] J.-G. Zhang, D. Wang, W. Xu, J. Xiao, R.E. Williford, J. Power Sources, 195 (2010) 4332-4337.

[14] N. Yan, G. Li, X. Gao, Journal of Materials Chemistry A, 1 (2013) 7012-7015.

[15] L. Li, A. Manthiram, Journal of Materials Chemistry A, 1 (2013) 5121-5127.

[16] F. Jaouen, E. Proietti, M. Lefèvre, R. Chenitz, J.-P. Dodelet, G. Wu, H.T. Chung, C.M. Johnston, P. Zelenay, Energy & Environmental Science, 4 (2011) 114-130.

[17] Y. Wang, H. Zhou, J. Power Sources, 195 (2010) 358-361.

[18] H. Zhou, Y. Wang, H. Li, P. He, ChemSusChem, 3 (2010) 1009-1019.

[19] H. Li, Y. Wang, H. Na, H. Liu, H. Zhou, J. Am. Chem. Soc., 131 (2009) 15098-15099.

[20] H. Li, Y. Wang, P. He, H. Zhou, Chem. Commun., 46 (2010) 2055-2057.

[21] C. Jia, F. Pan, Y.G. Zhu, Q. Huang, L. Lu, Q. Wang, Science advances, 1 (2015) e1500886.

[22] Y.G. Zhu, C. Jia, J. Yang, F. Pan, Q. Huang, Q. Wang, Chem. Commun., 51 (2015) 9451-9454.

[23] J. Christensen, P. Albertus, R.S. Sanchez-Carrera, T. Lohmann, B. Kozinsky, R. Liedtke, J. Ahmed, A. Kojic, J. Electrochem. Soc., 159 (2011) R1-R30.

[24] E. Kjeang, N. Djilali, D. Sinton, J. Power Sources, 186 (2009) 353-369.

[25] M.-A. Goulet, E. Kjeang, J. Power Sources, 260 (2014) 186-196.

[26] M. Nasharudin, S.K. Kamarudin, U.A. Hasran, M. Masdar, Int. J. Hydrogen. Energ, 39 (2014) 1039-1055.

[27] S.A.M. Shaegh, N.-T. Nguyen, S.H. Chan, Int. J. Hydrogen. Energ, 36 (2011) 5675-5694.

[28] L. Wang, F. Liu, W. Wang, G. Yang, D. Zheng, Z. Wu, M.K. Leung, RSC Advances, 4 (2014) 30857-30863.

[29] J.-B. Wang, J.-M. Wang, H.-B. Shao, J.-Q. Zhang, C.-N. Cao, J. Appl. Electrochem., 37 (2007) 753-758.

[30] L. Fan, H. Lu, J. Leng, Z. Sun, C. Chen, J. Power Sources, 299 (2015) 66-69.

[31] Z. Zhang, C. Zuo, Z. Liu, Y. Yu, Y. Zuo, Y. Song, J. Power Sources, 251 (2014) 470-475.

[32] L. Fan, H. Lu, J. Power Sources, 284 (2015) 409-415.

[33] Y. Li, M. Gong, Y. Liang, J. Feng, J.-E. Kim, H. Wang, G. Hong, B. Zhang, H. Dai, Nature communications, 4 (2013) 1805.

[34] K. Hayashi, K. Shima, F. Sugiyama, J. Electrochem. Soc., 160 (2013) A1467-A1472.

[35] B. Chen, D.Y. Leung, J. Xuan, H. Wang, Appl. Energ., (2015).

[36] B. Chen, D.Y. Leung, H. Wang, J. Xuan, J. Electrochem. Soc., 163 (2016) F1032-F1037.

[37] A. Abdel-Gaber, E. Khamis, H. Abo-ElDahab, S. Adeel, Mater. Chem. Phys., 109 (2008) 297-305.

[38] K. Emregül, A.A. Aksüt, Corros. Sci., 42 (2000) 2051-2067.

[39] A. Maghsodi, M.M. Hoseini, M.D. Mobarakeh, M. Kheirmand, L. Samiee, F. Shoghi, M. Kameli, Applied Surface Science, 257 (2011) 6353-6357.

[40] W. Ferrando, in, DTIC Document, 1987.

[41] D.D. Macdonald, Electrochim. Acta, 35 (1990) 1509-1525.

[42] C. Brett, J. Appl. Electrochem., 20 (1990) 1000-1003.

[43] N. Chaubey, V.K. Singh, M. Quraishi, International Journal of Industrial Chemistry, 6 (2015) 317-328.

[44] G. McLean, T. Niet, S. Prince-Richard, N. Djilali, Int. J. Hydrogen. Energ, 27 (2002) 507-526.

[45] S. Gryglewicz, Bioresource. Technol., 70 (1999) 249-253.

Figure 1 (a) Schematic of the hybrid electrolyte Al-air cell built on a non-direct counter-flow microfluidic platform. (b) Electrolyte flow pattern within the cell at a stream flow rate of (b1) 100 μL min^{-1} (b2) 300 μL min^{-1} (b3) 500 μL min^{-1} and (b4) 1000 μL min^{-1}. The contours reflect the water content inside the cell captured by a fluorescent microscope, flowing neat methanol and deionized water side by side. (c) Photograph of a hybrid electrolyte Al-air cell.

Figure 2 (a) Cell performance curves and (b) individual electrode polarization curves of the hybrid electrolyte Al-air cells with different KOH concentrations (Anolyte: neat methanol-based KOH solutions with KOH concentrations of 1 M, 2 M, 3 M and 4 M; Catholyte: aqueous KOH solution with KOH concentrations of 1 M, 2 M, 3 M and 4 M. (c) Cell performance curves and (d) individual electrode polarization curves of the hybrid electrolyte Al-air cells with different water content in the anolyte (Anolyte: 1 M KOH methanol-based solution with various water contents of 0 vol.%, 20 vol.%, 40 vol.% and 60 vol.%; Catholyte: 1 M KOH aqueous solution).

Figure 3 Specific capacities of Al foil in the hybrid electrolyte Al-air cells with (a) anolyte: neat methanol-based KOH solutions with KOH concentrations of 1 M, 2 M, 3 M and 4 M; catholyte: aqueous KOH solution with KOH concentrations of 1 M, 2 M, 3 M and 4 M. (b) anolyte: 1 M KOH methanol-based solution with various water contents of 0 vol.%, 20 vol.%, 40 vol.% and 60 vol.%; catholyte: 1 M KOH aqueous solution.

Figure 4 Impedance diagrams of the hybrid electrolyte Al-air cells with (a)anolyte: neat

methanol-based KOH solutions with KOH concentrations of 1 M, 2 M and 3 M; catholyte: aqueous KOH solution with KOH concentrations of 1 M, 2 M and 3 M; (b) anolyte: 1 M KOH methanol-based solution with various water contents of 20 vol.%, 40 vol.% and 100 vol.%; catholyte: 1 M KOH aqueous solution. (c) Schematic of an alkaline Al-air cell and its equivalent circuit.

Figure 5 SEM images of Al surface morphologies after discharging in (a) neat methanol-based and (b) water-based KOH anolyte. Insets are the corresponding sectional views of the Al electrodes.

Figure 6 XRD pattern of the precipitate on Al surface after discharging in KOH

Figure 7 FTIR spectra of the powder samples obtained from KOH methanol-based solution without/with Al discharge.